ELSEVIER

International Journal of Heat and Fluid Flow 21 (2000) 614–619

International Journal of HEAT AND FLUID FLOW

www.elsevier.com/locate/ijhff

Prediction of streamline curvature effects on wall-bounded turbulent flows

Nobuyuki Shima *, Takafumi Kawai, Masayoshi Okamoto, Ryuta Tsuchikura

Department of Mechanical Engineering, Shizuoka University, Johoku 3-5-1, Hamamatsu 432-8561, Japan

Abstract

A low-Reynolds-number second-moment closure without wall-reflection redistribution terms is tested in wall-bounded turbulent flows with streamline curvature. The turbulence model was previously shown to give good predictions for a fully developed channel flow, boundary layers in zero, adverse and favorable pressure gradients, plane and round jets, and flows with wall blowing and suction. In the present study, the model is used to calculate two fully developed curved channel flows and four boundary layers on curved walls. The turbulence model captures main features of the stabilizing and destabilizing effects of streamline curvature, though some notable discrepancies between the predictions and measurements are present in boundary layers on convex walls. © 2000 Begell House Inc. Published by Elsevier Science Inc. All rights reserved.

Keywords: Turbulence model; Second-moment closure; Streamline curvature; Channel flow; Boundary layer

1. Introduction

The "basic" second-moment turbulence closure (see Launder, 1989) and its low-Reynolds-number variants (e.g., Launder and Shima, 1989; Shima, 1993) have been widely used with success to calculate various turbulent flows. A weakness of these closures is that they contain wall-reflection redistribution terms, which are formulated using the wall distance and wall-normal vector. Due to these elements, it is difficult to apply the models to flows with complex wall geometries.

Recently, Shima (1998) proposed a low-Reynolds-number second-moment closure, which adopted a quasi-linear rapid redistribution model but eliminated the conventional wall-reflection redistribution terms. In that study, the model was tested in a fully developed channel flow, boundary layers in zero, adverse and favorable pressure gradients, and plane and round jets. The model performance was generally good. The closure was also successfully applied to wall-bounded flows with blowing and suction (Shima et al., 1999). These results encourage further testing of the model in various turbulent flows.

Turbulent flow with streamline curvature is of considerable engineering interest. Testing of turbulence models in a variety of such flows is clearly needed before a sufficiently general model is establihed. In the present study, we test the second-moment closure in two curved channel flows and four boundary layers on curved walls.

2. Turbulence model

In this section, the second-moment closure proposed by Shima (1998) is summarized. The stress transport model can be written as:

$$\frac{\mathrm{D}}{\mathrm{D}t}\overline{u_iu_j} = P_{ij} - \frac{2}{3}\varepsilon\delta_{ij} + \phi_{(1)ij} + \phi_{(2)ij} + T_{ij} + V_{ij}, \tag{1}$$

$$P_{ij} = -\left(\overline{u_ju_k}\frac{\partial U_i}{\partial x_k} + \overline{u_iu_k}\frac{\partial U_j}{\partial x_k}\right), \tag{2}$$

$$\phi_{(1)ij} = -C_1\frac{\varepsilon}{k}\left(\overline{u_iu_j} - \frac{2}{3}k\delta_{ij}\right), \tag{3}$$

$$\phi_{(2)ij} = -C_2\left(P_{ij} - \frac{2}{3}\delta_{ij}P\right) - C_3\left(D_{ij} - \frac{2}{3}\delta_{ij}P\right) - C_4k\left(\frac{\partial U_i}{\partial x_j} + \frac{\partial U_j}{\partial x_i}\right), \tag{4}$$

$$T_{ij} = \frac{\partial}{\partial x_k}\left(C_s\frac{k}{\varepsilon}\,\overline{u_ku_l}\,\frac{\partial\overline{u_iu_j}}{\partial x_l}\right), \tag{5}$$

$$V_{ij} = \nu\frac{\partial^2}{\partial x_k\partial x_k}\overline{u_iu_j}, \tag{6}$$

where U_i and u_i denote the mean and fluctuating velocity vectors, respectively, k the turbulence energy, ε its dissipation rate, ν the kinematic viscosity, and the overbar implies the ensemble averaging. In Eq. (4), $P = P_{kk}/2$ is the production rate of k, and

* Corresponding author. Tel.: +81-53-478-1055; fax: 81-53-478-1055.
E-mail address: tmnshim@ipc.shizuoka.ac.jp (N. Shima).

PII: S0142-727X(00)00052-7

$$D_{ij} = -\left(\overline{u_j u_k}\frac{\partial U_k}{\partial x_i} + \overline{u_i u_k}\frac{\partial U_k}{\partial x_j}\right). \tag{7}$$

The diffusion coefficient $C_s = 0.22$, and the four coefficients of redistribution terms are determined as:

$$C_1 = 1 + 2.45A_2^{1/4}A^{3/4}[1 - \exp\{-(7A)^2\}] \times [1 - \exp\{-(R_T/60)^2\}], \tag{8}$$

$$C_2 = 0.7A, \tag{9}$$

$$C_3 = 0.3A^{1/2}, \tag{10}$$

$$C_4 = 0.65A(0.23C_1 + C_2 - 1) + 1.3A_2^{1/4}C_3, \tag{11}$$

where A and A_2 are the invariants of the stress anisotropy tensor $a_{ij} = \overline{u_i u_j}/k - 2\delta_{ij}/3$ defined by:

$$A = 1 - 9A_2/8 + 9A_3/8, \tag{12}$$

$$A_2 = a_{ij}a_{ji}, \tag{13}$$

$$A_3 = a_{ij}a_{jk}a_{ki}, \tag{14}$$

and $R_T = k^2/v\varepsilon$ is the turbulence Reynolds number.

The transport model for ε is

$$\frac{D\varepsilon}{Dt} = C_{\varepsilon 1}\frac{\varepsilon}{k}P - C_{\varepsilon 2}\frac{\varepsilon\tilde{\varepsilon}}{k} + \frac{\partial}{\partial x_k}\left(C_\varepsilon \frac{k}{\varepsilon}\overline{u_k u_l}\frac{\partial \varepsilon}{\partial x_l} + v\frac{\partial \varepsilon}{\partial x_k}\right), \tag{15}$$

where

$$\tilde{\varepsilon} = \varepsilon - 2v\left(\frac{\partial k^{1/2}}{\partial x_l}\right)^2. \tag{16}$$

The coefficients $C_{\varepsilon 2}$ and C_ε are assigned standard values, i.e., $C_{\varepsilon 2} = 1.92$ and $C_\varepsilon = 0.15$. For the coefficient $C_{\varepsilon 1}$, the form

$$C_{\varepsilon 1} = 1.44 + \beta_1 + \beta_2, \tag{17}$$

$$\beta_1 = 0.25A\min(\lambda/2.5 - 1,\ 0) - 1.4A\min(P/\varepsilon - 1,\ 0), \tag{18}$$

$$\beta_2 = 1.0A\lambda^2\max(\lambda/2.5 - 1,\ 0), \tag{19}$$

$$\lambda = \min(\lambda^*, 4), \tag{20}$$

$$\lambda^* = \left[\frac{\partial}{\partial x_i}\left(\frac{k^{3/2}}{\varepsilon}\right)\frac{\partial}{\partial x_i}\left(\frac{k^{3/2}}{\varepsilon}\right)\right]^{1/2} \tag{21}$$

is adopted.

In the present stress transport model, the conventional wall-reflection redistribution terms have been eliminated. The rapid term with C_3 works to produce the high anisotropy in normal stresses in the wall vicinity. In thin shear flows, the C_4 term appears only in the shear stress transport equation, and the form (11) has been designed to reproduce a shear stress behavior in the log layer. For more details of the closure, see Shima (1998).

3. Test cases

Table 1 summarizes the test cases. In curved channel flows (Cases 1 and 2), δ denotes the channel half-width, and R is the radius of curvature of the channel centerline. For boundary layers (Cases 3–6), δ denotes the boundary layer thickness, and R is the radius of curvature of the wall. Case 1 is a fully developed flow in a circularly curved channel, which Moser and Moin (1987) created by direct numerical simulation (DNS). In this case, the curvature is mild. Case 2 is also a fully developed curved channel flow from Kobayashi et al. (1989) experiment in which the curvature is stronger than in Case 1. Cases 3–6 are boundary layer flows on curved walls taken from well-known experimental investigations. In Cases 3 and 4 (Hoffmann and Bradshaw), the curvature is mild, while Case 5 (Gillis and Johnston, 1980) and Case 6 (Alving et al., 1990) are strongly curved flows. Cases 5 and 6 include recovery flow on a flat wall downstream of the curved section. The experimental data of Cases 3, 4 and 6 are obtained from CTTM Data Library (1993).

In Cases 1–3, due to instabilities associated with concave curvature, Taylor–Görtler vortices may exist. In the experiment of Case 2, the authors observed no longitudinal vortices, while in Cases 1 and 3, Taylor–Görtler vortices are present and the statistics vary in the spanwise direction. However, we make one-dimensional calculation for Case 1 as well as Case 2, and two-dimensional calculation for Case 3, as suggested for Case 3 at the 1980–1981 Stanford Conference (Kline et al., 1981).

In the case of fully developed curved channel flows, the governing equations in cylindrical coordinates r–θ–z reduce to a set of ordinary differential equations. The equations were discretized by a second-order accurate finite-volume approach and then solved by an iterative method. The number of grid points was 140, concentrated towards the wall. Grid independence was confirmed by using a 70-point grid without any perceptible effect on the results.

In case of boundary layer, the governing equations to be solved are obtained by applying the boundary layer approximation to the mean flow and turbulence model equations expressed in a coordinate system whose abscissa x is measured along the wall, the ordinate y being measured at right angles to it. The numerical solutions were obtained with an adapted version of the parabolic solver PASSABLE (Leschziner, 1982). For the solution procedure, see Launder and Shima (1989) and Shima (1993).

4. Results

Fig. 1 compares the second-moment closure (denoted by Sh model) with DNS data for fully developed curved channel flow at $U_c\delta/v = 2990$ (Case 1), where U_c is the centerline velocity. In Fig. 1(a), the mean velocity in the streamwise direction U and the distance from the wall y are non-dimensionalized with local friction velocities. In Figs. 1(b) and (c), U_τ denotes the global friction velocity defined by analogy with the plane channel

Table 1
Test cases

Case	Investigators	Flow type	δ/R
1	Moser and Moin	Curved channel flow	$= 0.0127$
2	Kobayashi et al.	Curved channel flow	$= 0.0417$
3	Hoffmann and Bradshaw	Boundary layer on concave wall	$\simeq 0.01$
4	Hoffmann and Bradshaw	Boundary layer on convex wall	$\simeq 0.01$
5	Gillis and Johnston	Boundary layer on convex wall	$\simeq 0.1$
6	Alving et al.	Boundary layer on convex wall	$\simeq 0.1$

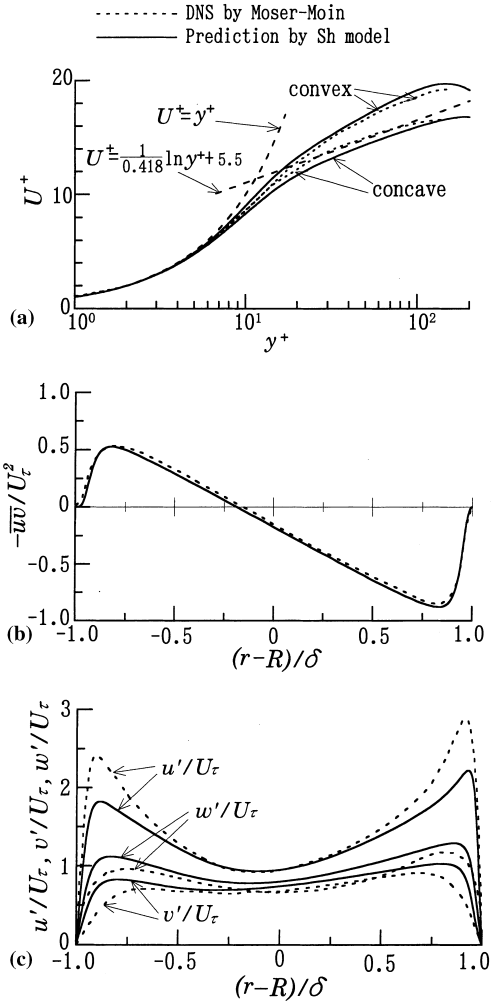

Fig. 1. Curved channel flow (Case 1): (a) mean velocity in wall coordinates; (b) shear stress; (c) turbulence intensities.

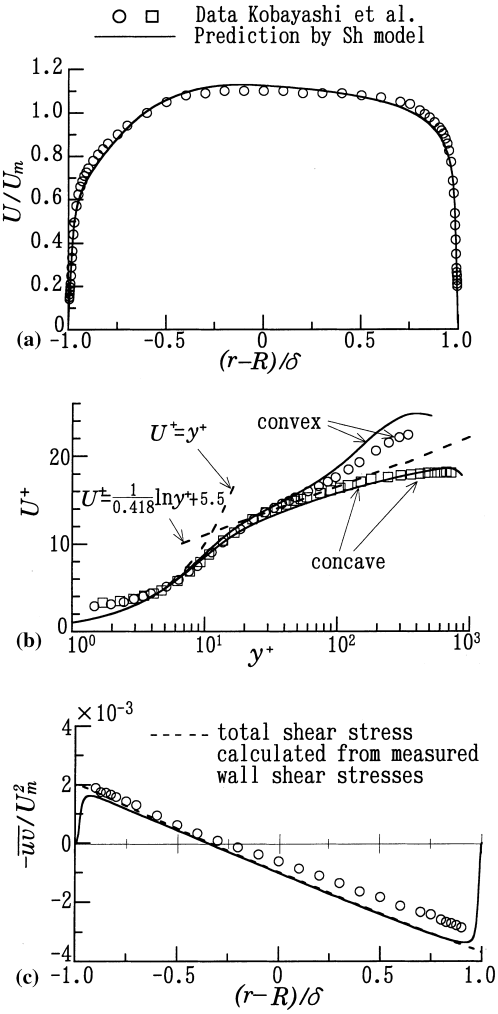

Fig. 2. Curved channel flow (Case 2): (a) mean velocity; (b) mean velocity in wall coordinates; (c) shear stress.

using the pressure gradient. The locations $(r-R)/\delta = -1$ and 1 correspond to the convex and concave walls, respectively. Reynolds numbers based on the predicted local friction velocities and δ are 153 at the convex side and 178 at the concave side, close to DNS values, 155 and 180, respectively. As is seen, the mean velocity and shear stress profiles are reproduced well by the prediction, though the difference between convex-side and concave-side velocity profiles is somewhat overpredicted. For the turbulence intensities, the model properly yields asymmetric profiles, but does not reproduce the high anisotropy in the wall vicinity, as expected from the result for plane channel flow (Shima, 1998).

Fig. 2 shows the performance in the curved channel flow with stronger curvature at $U_m\delta/\nu = 10000$ (Case 2), where U_m is the bulk mean velocity. Reynolds numbers based on the predicted local friction velocities are 456 at the convex side and 596 at the concave side, somewhat lower than DNS values, 487 and 606, respectively. As is seen from Fig. 2(a), the present model captures the stabilizing and destabilizing effects of curvature, giving an asymmetric velocity profile close to the experimental data. When plotted in wall coordinates (Fig. 2(b)), the predicted convex-side profile lies above the measured profile due to the underpredicted skin friction, indicating that the model somewhat overpredicts the stabilizing effect of convex curvature. In Fig. 2(c), the calculated shear stress deviates appreciably from the experimental data. The figure includes a total shear stress distribution calculated from measured wall shear stresses, which is not fully consistent with the measured Reynolds shear stress. Therefore, the disagreement between the prediction and data in Fig. 2(c) is not conclusive.

In the fully developed flow in a circularly curved channel, the shear stress transport equation can be written as

$$\begin{aligned}\left(\overline{v^2}-\overline{u^2}\right)\frac{U}{r} = & -\overline{v^2}\frac{\partial U}{\partial r}+\overline{u^2}\frac{U}{r}-C_1\frac{\varepsilon}{k}\overline{uv}\\ & +C_2\left(\overline{v^2}\frac{\partial U}{\partial r}-\overline{u^2}\frac{U}{r}\right)-C_3\left(\overline{v^2}\frac{U}{r}-\overline{u^2}\frac{\partial U}{\partial r}\right)\\ & -C_4kr\frac{\partial}{\partial r}\left(\frac{U}{r}\right)+\frac{1}{r}\left[\frac{\partial}{\partial r}\left\{r\left(C_s\frac{k}{\varepsilon}\overline{v^2}+\nu\right)\frac{\partial\overline{uv}}{\partial r}\right\}\right.\\ & \left.+\frac{\partial}{\partial r}\left\{C_s\frac{k}{\varepsilon}\overline{uv}\left(\overline{v^2}-\overline{u^2}\right)\right\}+C_s\frac{k}{\varepsilon}\overline{uv}\frac{\partial}{\partial r}\left(\overline{v^2}-\overline{u^2}\right)\right.\\ & \left.-4\left(C_s\frac{k}{\varepsilon}\overline{u^2}+\nu\right)\frac{\overline{uv}}{r}\right],\end{aligned} \tag{22}$$

where u and v denote the velocity fluctuation components in the θ and r directions, respectively, and U is the mean velocity component in the θ direction. The exact curvature-related production $\overline{u^2}U/r$ and the exact convection $(\overline{v^2}-\overline{u^2})U/r$ on the left-hand side act to reduce and augment the shear stress

magnitude near the convex ($\overline{uv} < 0$) and concave ($\overline{uv} > 0$) walls, respectively. The good predictions presented above are mainly due to these exact terms, though, of course, the redistribution modeling is important for accurate predictions.

We now turn to boundary layer flows. For brevity, the governing equations in the adopted coordinate system are not shown; the curvature-related stress convection, production and redistribution terms are essentially the same as those in curved channel flow. The result for the case of mild concave curvature (Case 3) is shown in Fig. 3, where U_p denotes the potential flow velocity, U_{pw} is U_p at the wall, and the skin friction coefficient is defined by $C_f = 2\tau_w/\rho U_{pw}^2$ (where τ_w is the wall shear stress and ρ is the density). A prediction using another low-Reynolds-number second-moment closure (denoted by LS* model), which adopts the wall-reflection redistribution terms is also plotted for comparison. This closure is a slightly modified version (Shima, 1993) of the model proposed by Launder and Shima (1989). For completeness, the LS* model is given in Appendix A. The response of the boundary layer to the applied concave curvature is rather slow (see Hoffmann et al., 1985). As is seen from Fig. 3(c), a high shear stress region grows gradually in the outer layer with increasing streamwise distance, due to the destabilizing effect of the concave curvature. At the last measurement station, the region is very wide. The Sh model captures this behavior, while the LS* model does not. As shown in Fig. 3(a), the skin friction also increases appreciably in the streamwise direction, and the Sh model predicts the experimental variation well. The mean velocity profiles are also reproduced faithfully by the model.

Fig. 4 compares the predictions with experimental data for Case 4. In this case, the effect of curvature on skin friction coefficient is less evident than in Case 3, but in the outer layer, the mild convex curvature appreciably reduces the shear stress. The shear stress profiles at four stations are shown in Fig. 4(c). At Station 2, just after the start of convex curvature, the outer layer quickly responds to the curvature, and the shear stress decreases considerably. This quick response contrasts with the relatively slow response to concave curvature in Case 3 (see Muck et al., 1985). The prediction with the Sh model captures this quick response, but gives an excessively large reduction.

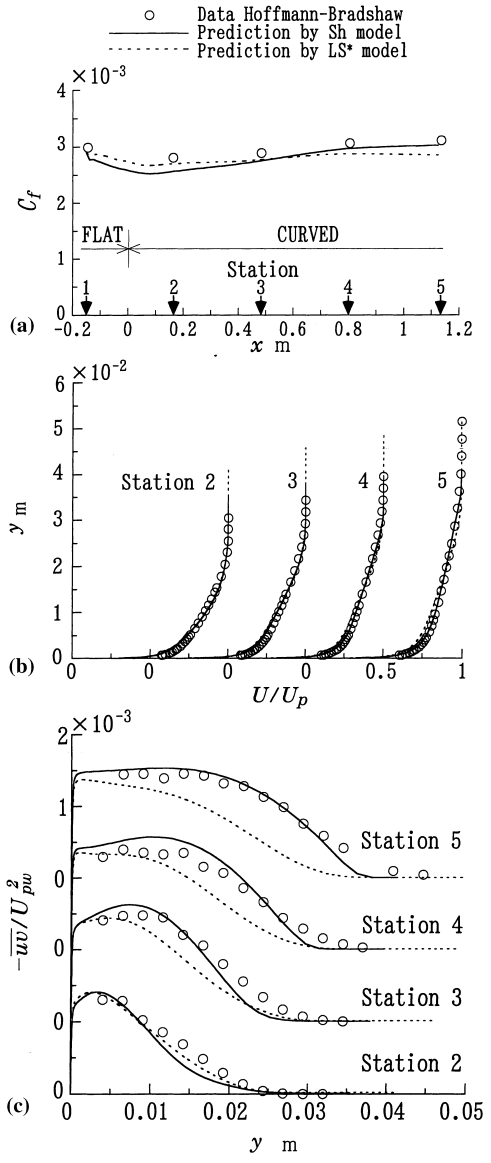

Fig. 3. Boundary layer on concave wall (Case 3): (a) skin friction coefficient; (b) mean velocity; (c) shear stress.

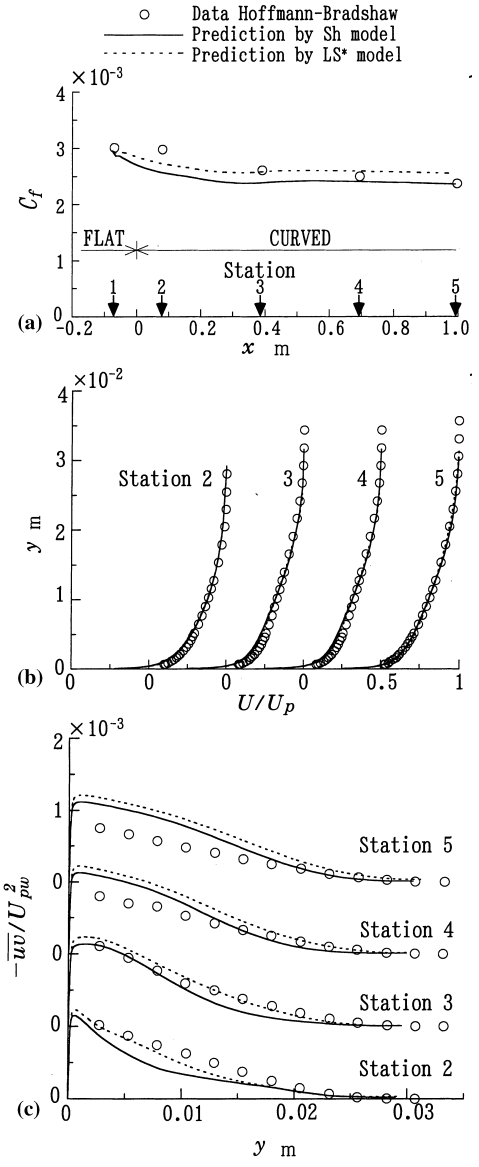

Fig. 4. Boundary layer on convex wall (Case 4): (a) skin friction coefficient; (b) mean velocity; (c) shear stress.

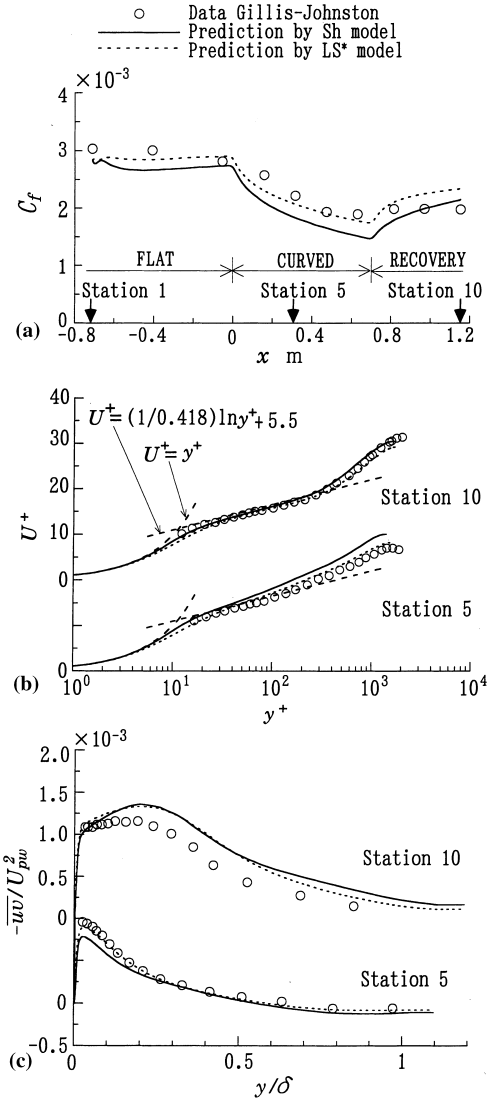

Fig. 5. Boundary layer on convex wall and recovery flat wall (Case 5): (a) skin friction coefficient; (b) mean velocity in wall coordinates; (c) shear stress.

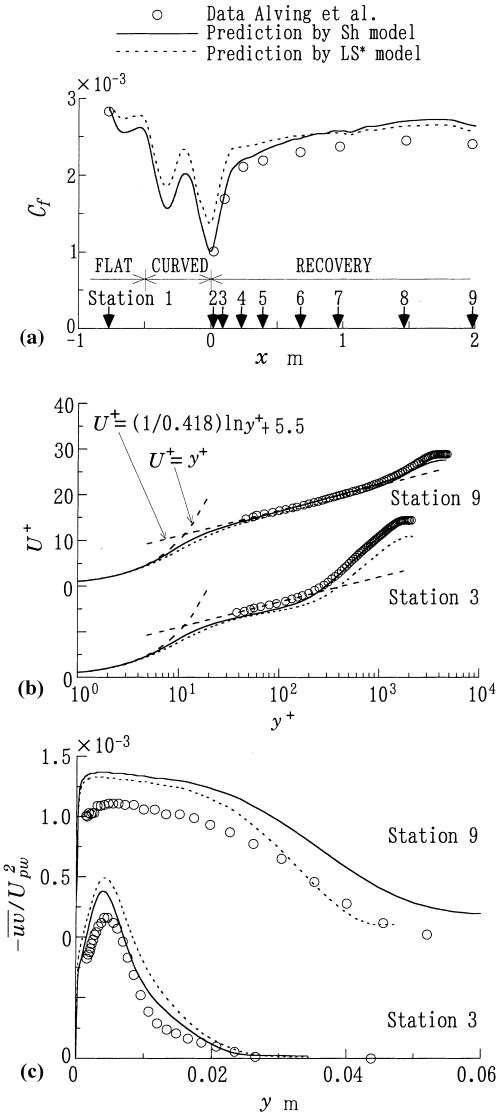

Fig. 6. Boundary layer on convex wall and recovery flat wall (Case 6): (a) skin friction coefficient; (b) mean velocity in wall coordinates; (c) shear stress.

The predicted shear stress then increases downstream, whereas the experimental data show a slow decrease. As is seen from Figs. 4(a) and (b), the Sh model slightly underpredicts the skin friction coefficient, and gives good predictions for mean velocity profiles.

Fig. 5 shows the comparison between measurements and predictions for Case 5. The two models capture the marked reduction in skin friction in the highly curved section, but the Sh model gives an excessively large reduction. This is consistent with the predicted mean velocity profile at Station 5, which lies above the measured profile. In the shear stress profile at this station, the Sh model reproduces well the profile in the outer layer including a negative stress region, but underpredicts the peak value near the wall, leading to low value of C_f. The very slow recovery in the experiment is not captured by either of the two models. In this case, the overall prediction with the LS* model is closer to measurements than that with the Sh model.

Finally, the streamwise variation of skin friction coefficient and the mean velocity and shear stress profiles for Case 6 are shown in Fig. 6. This experiment concentrates on the recovery from strong convex curvature, and no measurements are available in the curved section except pressure distributions. In the curved section, steep positive and negative pressure gradients exist, and the predicted skin friction varies in a complex manner under the effects of curvature and pressure gradient. In this strongly curved section, the Sh model seems to give better prediction than the LS* model, in contrast to Case 5. At Station 3, just after the removal of wall curvature, the large wake component in the measured velocity profile is reproduced well, and the predicted C_f agrees well with the experimental value. At this station, however, the peak value of the shear stress is overpredicted, Fig. 6(c). This leads to a large skin friction in the recovery and a high level of shear stress at the last measurement station.

5. Concluding remarks

A second-moment closure without wall-reflection redistribution terms has been tested in six different wall-bounded

flows with streamline curvature. On the whole, the turbulence model with no curvature-specific modifications captures main features of the stabilizing and destabilizing effects of streamline curvature. As expected, the elimination of wall-reflection redistribution terms does not cause difficulties in predicting the effects of streamline curvature. In boundary layers on convex walls, some notable discrepancies between the predictions and measurements are present. We feel that it is possible to obtain better predictions by refining model functions in the redistribution term and in the dissipation-rate transport equation.

Appendix A. LS* model

In the stress transport equation

$$\frac{\mathrm{D}}{\mathrm{D}t}\overline{u_i u_j} = P_{ij} - \frac{2}{3}\varepsilon\delta_{ij} + \phi_{ij} + T_{ij} + V_{ij},$$

the redistribution model ϕ_{ij} is:

$$\phi_{ij} = \phi_{(1)ij} + \phi_{(2)ij} + \phi_{(\mathrm{w}1)ij} + \phi_{(\mathrm{w}2)ij},$$

$$\phi_{(1)ij} = -C_1\frac{\varepsilon}{k}\left(\overline{u_i u_j} - \frac{2}{3}\delta_{ij}k\right),$$

$$\phi_{(2)ij} = -C_2\left(P_{ij} - \frac{2}{3}\delta_{ij}P\right),$$

$$\phi_{(\mathrm{w}1)ij} = C_{\mathrm{w}1}\frac{\varepsilon}{k}\left(\overline{u_k u_m}n_k n_m\delta_{ij} - \frac{3}{2}\overline{u_k u_i}n_k n_j - \frac{3}{2}\overline{u_k u_j}n_k n_i\right)\frac{k^{3/2}}{C_l\varepsilon d},$$

$$\phi_{(\mathrm{w}2)ij} = C_{\mathrm{w}2}\left(\phi_{(2)km}n_k n_m\delta_{ij} - \frac{3}{2}\phi_{(2)ik}n_k n_j - \frac{3}{2}\phi_{(2)jk}n_k n_i\right)\frac{k^{3/2}}{C_l\varepsilon d},$$

$$C_1 = 1 + 2.58AA_2^{1/4}[1 - \exp\{-(0.0067R_{\mathrm{T}})^2\}],$$

$$C_2 = 0.75A^{1/2},$$

$$C_{\mathrm{w}1} = -2C_1/3 + 1.67,$$

$$C_{\mathrm{w}2} = \max[2(C_2 - 1)/3 + 0.5,\ 0]/C_2.$$

The terms $\phi_{(\mathrm{w}1)ij}$ and $\phi_{(\mathrm{w}2)ij}$ with $C_l = 2.5$ are wall-reflection redistributions, which are formulated using the wall distance d and wall-normal vector n_i. The turbulent diffusion T_{ij} is the same as that in the Sh model.

In the ε transport equation (15), the LS* model adopts:

$$C_{\varepsilon 1} = 1.45 + \psi_1 + \psi_2,$$

$$\psi_1 = 1.5A(P/\varepsilon - 1),$$

$$\psi_2 = 0.35(1 - 0.3A_2)\exp[-(0.002R_{\mathrm{T}})^{1/2}],$$

$$C_{\varepsilon 2} = 1.9, \quad C_{\varepsilon} = 0.18.$$

The LS* model differs from the closure proposed by Launder and Shima (1989) only in the constants in the model functions ψ_1 and ψ_2. For more details, see Shima (1993).

References

Alving, A.E., Smits, A.J., Watmuff, J.H., 1990. Turbulent boundary layer relaxation from convex curvature. J. Fluid Mech. 211, 529–556.

Collaborative Testing of Turbulence Models (CTTM) Data Library, 1993. Mechanical Engineering Department, Stanford University.

Gillis, J.C., Johnston, J.P., 1980. Experiments on the turbulent boundary layer over convex walls and its recovery to flat-wall conditions. In: Bradbury, L.J.S., et al. (Eds.), Turbulent Shear Flows 2. Springer, New York, pp. 116–128.

Hoffmann, P.H., Muck, K.C., Bradshaw, P., 1985. The effect of concave surface curvature on turbulent boundary layers. J. Fluid Mech. 161, 371–403.

Kline, S.J., Cantwell, B.J., Lilley, G.M. (Eds.), 1981. Proceedings of the 1980–1981 AFOSR-HTTM-Stanford Conference on Complex Turbulent Flows.

Kobayashi, M., Maekawa, H., Takano, T., Uchiyama, N., Kubota, M., Kobayashi, Y., 1989. Two-dimensional turbulent flow in a curved channel. JSME Int. J. Series II 32, 324–331.

Launder, B.E., 1989. Phenomenological modelling: present... and future? In: Lumley, J.L. (Ed.), Whither Turbulence? Turbulence at the Crossroads. Springer, New York, pp. 439–485.

Launder, B.E., Shima, N., 1989. Second-moment closure for the near-wall sublayer: development and application. AIAA J. 27, 1319–1325.

Leschziner, M.A., 1982. An introduction and guide to PASSABLE. Thermofluids Division, Department of Mechanical Engineering, UMIST.

Moser, R.D., Moin, P., 1987. The effects of curvature in wall-bounded turbulent flows. J. Fluid Mech. 175, 479–510.

Muck, K.C., Hoffmann, P.H., Bradshaw, P., 1985. The effect of convex surface curvature on turbulent boundary layers. J. Fluid Mech. 161, 347–369.

Shima, N., 1993. Prediction of turbulent boundary layers with a second-moment closure: Parts I and II. ASME J. Fluids Eng. 115, 56–69.

Shima, N., 1998. Low-Reynolds-number second-moment closure without wall-reflection redistribution terms. Int. J. Heat Fluid Flow 19, 549–555.

Shima, N., Saito, N., Okamoto, M., 1999. Prediction of wall-bounded turbulent flows with blowing and suction. JSME Int. J. Series B 42, 626–633.